www.czasopisma.pan.pl PAN POLSKA AKADEMIA NAUK www.journals.pan.pl
Chemical and Process Engineering 2015, 36 (2), 251-262
DOI: 10.1515/cpe-2015-0017

COMPARISON OF LARGE EDDY SIMULATIONS AND k-ε MODELLING OF FLUID VELOCITY AND TRACER CONCENTRATION IN IMPINGING JET MIXERS

Krzysztof Wojtas*, Wojciech Orciuch, Łukasz Makowski

Warsaw University of Technology, Faculty of Chemical and Process Engineering, Warynskiego Street 1, 00-645 Warsaw, Poland

Simulations of turbulent mixing in two types of jet mixers were carried out using two CFD models, large eddy simulation and k-ε model. Modelling approaches were compared with experimental data obtained by the application of particle image velocimetry and planar laser-induced fluorescence methods. Measured local microstructures of fluid velocity and inert tracer concentration can be used for direct validation of numerical simulations. Presented results show that for higher tested values of jet Reynolds number both models are in good agreement with the experiments. Differences between models were observed for lower Reynolds numbers when the effects of large scale inhomogeneity are important.

Keywords: jet mixers, mixing, PIV, PLIF, LES

1. INTRODUCTION

Turbulent mixing of liquids is commonly used in industrial processes, especially in those with fast parallel chemical reactions, where mixing efficiency, expressed as micromixing time, plays a crucial role in obtaining a high-quality product. In such applications impinging jets mixers are often used, because they enable almost instantaneous mixing at the molecular level of contacting liquids (Johnson and Prud'homme, 2003). This is related to formation of high values of the rate of energy dissipation in impingement zone of inlet streams. Since energetic cost per volumetric flow of the product in this type of mixers is high compared to other solutions (Kölbl et al., 2011), many literature works have been devoted to designing more efficient jet mixer geometries (Liu et al., 2008; Marchisio, 2009). The main application of jet mixers can be found in pharmaceutical (Johnson and Prud'homme, 2003; Lince et al., 2008), catalytic (Marchisio, 2009; Midler et al., 1994) and fluid lubricants industries for nanoparticle production (Santillo et al., 2012).

Since the design process of the new chemical reactor using only experiments can be difficult and expensive, one can utilise hydrodynamics simulations with computational fluid dynamics (CFD). However, when CFD simulations of turbulent flows in jet mixers are considered, two flow regimes can coexist in such systems (Tamir, 1994). In the impingement zone of inlet streams a highly turbulent flow occurs, while in other parts laminar flow can be observed. Under such conditions, widely used Reynolds-Averaged Navier Stokes (RANS) models lead very often to poor predictions (Icardi et al., 2011; Makowski and Bałdyga, 2011; Makowski et al., 2012; Schwertfirm and Manhart, 2010).

*Corresponding author, e-mail: k.wojtas@ichip.pw.edu.pl

Therefore investigations of velocity and concentration distribution inside mixers are very important to validate CFD models, especially time-dependent models like large eddy simulations (LES).

2. EXPERIMENTAL SYSTEM

In this work the authors investigated the course of mixing process in two types of jet mixers (Figure 1) which were selected to determine the influence of inlet velocity, jet Reynolds numbers and asymmetry of the inlet pipes on mixing process. Both mixers are typical T-mixers, and each type of mixer was studied in two variants: with inlet pipes of diameter, d_{jet}, equal to 4.6 mm or 7 mm. The outlet pipe diameter, d_{out}, was constant in each mixer and was equal to 11 mm. Symmetric mixers can be characterised by symmetrically arranged inlet pipes to the mixing chamber, whereas vortex mixers have inlet pipes arranged tangentially to the outlet pipe. The lengths of inlet pipes were equal to 100 mm and the length of outlet pipes was equal to 300 mm. Since several jet mixers were studied, therefore, for the sake of readability they will be further referred to as:

- T-mixer I - symmetric mixer with $d_{jet} = 7$ mm;
- T-mixer II - symmetric mixer with $d_{jet} = 4.6$ mm;
- V-mixer I - vortex mixer with $d_{jet} = 7$ mm;
- V-mixer II - vortex mixer with $d_{jet} = 4.6$ mm.

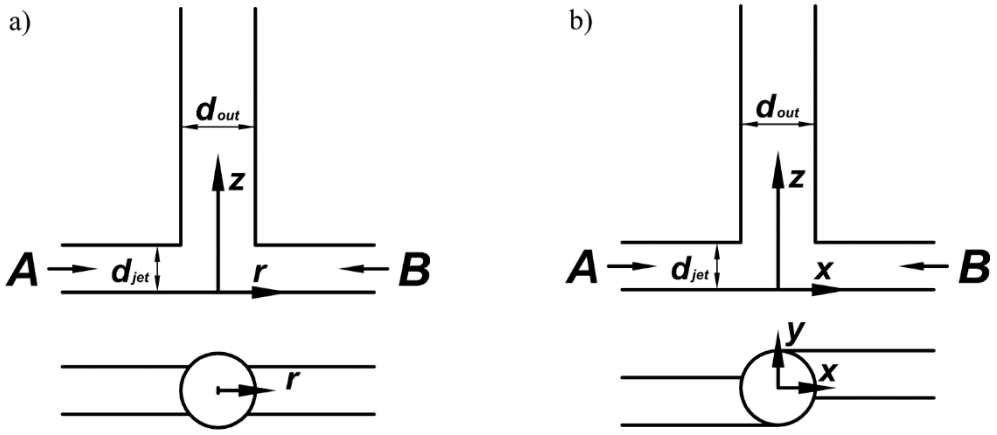

Fig. 1. Geometry of the mixers: a) T-mixer, b) V-mixer

Experiments were carried out using two measurement techniques: particle image velocimetry (PIV) and planar laser-induced fluorescence (PLIF). These techniques were applied to obtain instantaneous distributions of fluid velocity and tracer concentration respectively. The measurement system consisted of a double-cavity Nd-YAG 532 nm laser with energy equal to 50 mJ per pulse and two CCD cameras (double frame Dantec Dynamics FlowSense 4M, 12 bits, 2048 x 2048 resolution; single frame Dantec Dynamics HiSense MkII, 12 bits, 1344 x 1024 resolution). The cameras were equipped with Nikon AF Micro 60 mm lens (aperture range from f/2.8 to f/32) provided with macro rings in order to further increase magnification. In order to increase sharpness across the frame and to reduce optical distortion effects, images were taken at the minimum aperture value and experimental systems were equipped with a transparent rectangular casing which was filled with double distilled water during measurements. The casing was also used as a thermostat and thereby constant temperature during measurements was obtained (293 K). With the use of cylindrical lenses laser beam was transformed to a collimated planar laser sheet. Laser sheet was crossing the experimental system vertically through the axis of the outlet pipe up from the bottom of the system (Figure 2). Thickness of a laser sheet in PIV and PLIF experiments plays an important role in microscale measurements (Mortensen et al., 2004). The spatial resolution of the experiments resulted from camera resolution and the laser thickness equal to 0.2 mm. In case of PIV the spatial resolution was about 10^{-3} mm^3, while in PLIF experiments it was between

10^{-5} and 10^{-4} mm^3. An order of the spatial resolution volume magnitude is similar (or even smaller) than the volume of a cell in the fine CFD meshes. Therefore, collected experimental data can be directly compared to the CFD results. Dantec borosilicate glass particles of density 2230 kg m^{-3} and average size equal to 10 µm were used as seeding particles for PIV measurements. Particles were equally dispersed in the inlet solutions. Rhodamine B was used as a fluorescent tracer in PLIF measurements and its concentration in the inlet solution, c_{in}, was equal to 0.2 g m^{-3}. In order to eliminate optical interferences in PLIF experiments, the camera was equipped with an optical filter which passes light having a wavelength similar to the wavelength of light emitted by Rhodamine B (610 nm).

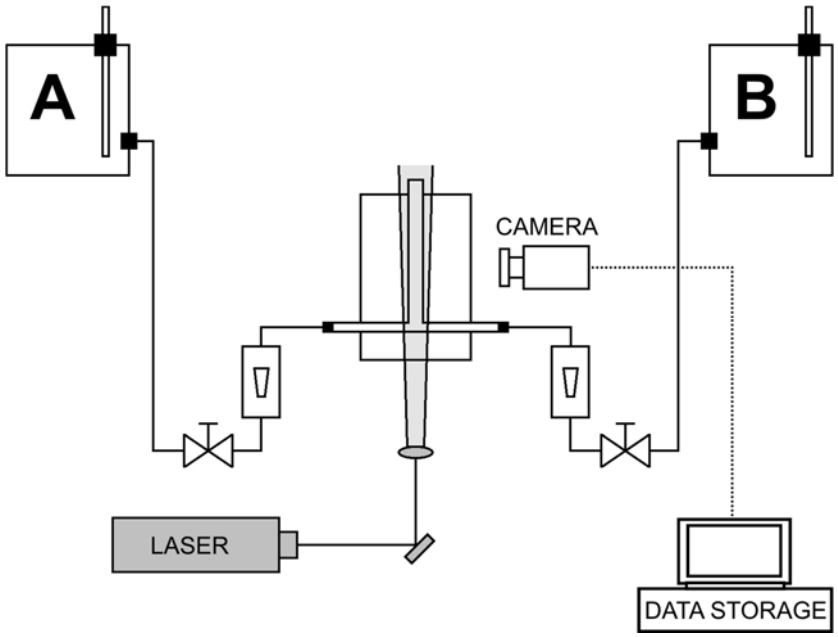

Fig. 2. Schematic diagram of experimental system

In all experiments all solutions were prepared from double distilled water. In PIV experiments streams A and B contained seeding particles, while in PLIF measurements stream A was water and stream B contained also Rhodamine B. To achieve a steady flow of solutions, two tanks working as Mariotte's bottles were installed above the experimental system as sources of solutions, while the flow rate was controlled with the use of rotameters and precise poppet valves.

Velocity vector maps were calculated using PIV software (Dantec Dynamics Studio) with "Adaptive correlation" procedure to minimise systematic errors. The initial interrogation area was set to 128 px x 128 px and the final interrogation area was 16 px x 16 px and the areas did not overlap. The number of refinements as well as the number of initial, intermediate and final steps, were set to 3. Each frame was 18 mm x 18 mm with a resolution of about 9 µm per px. The time between laser pulses was set according to mean flow rate, and was in the range from 125 µs, for the highest tested Reynolds number, to 500 µs. The time between laser pulses and interrogation area was chosen such that the maximum displacement between frames was less than half of the interrogation area size.

During experiments a value of local instantaneous mixture fraction, f, was determined, which resulted from local instantaneous value of rhodamine concentration, c, measured by PLIF:

$$f = \frac{c}{c_{in}} \tag{1}$$

The experimentally determined values of the variance for each measured point were calculated from:

$$\sigma^2 = \int_0^1 [f - \langle f \rangle]^2 \phi(f) df = \frac{1}{N} \sum_{i=1}^{N} [f_i - \langle f \rangle]^2 \tag{2}$$

where $\phi(f)$ represents the probability density function (PDF) and N is the number of two-dimensional maps. PIV and PLIF experiments were repeated three times to obtain average results.

3. SIMULATIONS

Simulations of hydrodynamics were carried out using CFD software Ansys Fluent 14. The computational domain was created in ANSYS ICEM 14 and the numerical mesh consisted of about 800 000 hexahedral cells for each mixer, with the average filter width, $\bar{\Delta}$, in the impingement zone equal to about 10^{-3} mm^3. The grid was the densest in the regions where large gradients of velocity and concentrations were predicted, i.e. in the impingement zone. It was checked that the results of computations were not sensitive to a further increase of the number of cells. The SIMPLE method was used for the pressure-velocity coupling, and higher-order discretisation schemes were used for all variables to minimise numerical diffusion effects. Computations were regarded as satisfactory converged when the total normalised residuals were smaller than 10^{-6}. The mean values of all simulated parameters in LES were obtained using a time-averaging with time interval taken as 10 τ, where τ represents the mean residence time in the mixer (the range of mean residence time was from 0.7 s to 2.8 s, while mean residence time in the impinging zone was from 0.04 s to 0.16 s), whereas the time step was equal to 1/100 τ.

Two turbulence models were used: the realizable k-ε model with enhanced wall treatment function and the large eddy simulation in which Smagorinsky-Lilly dynamic stress model was employed to reflect the effects of the small scale on large ones. The distribution of the filtered mean mixture fraction, $\bar{f}$, for LES was described using the gradient diffusion approximation:

$$\frac{\partial \bar{f}}{\partial t} + \bar{u}_i \frac{\partial \bar{f}}{\partial x_i} = \frac{\partial}{\partial x_i}\left[\left(D_m + D_{sgs}\right)\frac{\partial \bar{f}}{\partial x_i}\right] \tag{3}$$

where D_m is molecular diffusivity and D_{sgs} is subgrid diffusivity. The well-known model based on the subgrid Schmidt number was applied to determine the values of subgrid diffusivity (Pitsch and Steiner, 2000):

$$Sc_{sgs} = \frac{\nu_{sgs}}{D_{sgs}} = 0.4 \tag{4}$$

where ν_{sgs} is subgrid viscosity.

Local values of mixture fraction variance are necessary to determine segregation defined by intensity of segregation. Note that the values of intensity of segregation equal to 0 indicate of ideal mixing in a molecular scale, whereas values of 1 mean perfect segregation. Information about mixture fraction variance and intensity of segregation allows to predict the course of complex processes.

To predict subgrid concentration variance, $\overline{\sigma_{sgs}^2}$, the scale-similarity model (Cook and Riley, 1994) was used, which uses the self-similar behavior of turbulent properties at different wave numbers. Based on the assumption of the fractal nature of turbulence, the subgrid scale variance can be determined using slightly larger scales. The scalar variance is then expressed as:

$$\overline{\sigma_{sgs}^2} \approx c_L \widetilde{\sigma_{sgs}^2} = c_L\left(\widetilde{\bar{f}^2} - \tilde{\bar{f}}^2\right) \tag{5}$$

where $\tilde{}$ denotes the test-filter and c_L is the model constant that needs to be specified. In the present work the test-filter that is twice the filter width ($\tilde{\bar{\Delta}} = 2\bar{\Delta}$, where $\bar{\Delta}$ corresponds to numerical grid size) was used.

Cook and Riley (1994) showed that model mentioned above yielded accurate predictions in homogeneous isotropic turbulence. In turbulent mixing of liquids, viscous-convective subrange on the

energy spectrum of the fluctuations of concentration occurs at scales below the Kolmogorov scale due to the high value of the Schmidt number (Bałdyga and Bourne, 1999). Michioka and Komori (2004) using direct numerical simulation results identified that with the increase of the Schmidt number, a constant value of c_L increases reaching an asymptotic value of 5.

The computational cost of LES is much higher than that of widely used RANS models, therefore, in practical applications LES should be used for solving problems in which simpler, and faster RANS models fail. For that reason, LES results employing the SGS models were compared with the results of RANS modeling (k-ε) supplemented with the non-equilibrium multiple-time-diffusion model - Turbulent Mixer Model (TMM) (Bałdyga, 1989; Bałdyga and Bourne, 1999), which enables prediction of the distribution of concentration variance.

4. RESULTS AND DISCUSSION

The experiments and calculations were performed for Re_{jet} equal to 1000, 2000 and 4000, where

$$Re_{jet} = \frac{u_{jet} d_{jet} \rho}{\mu} \tag{6}$$

and u_{jet} is mean velocity at the inlet, ρ and μ are density and dynamic viscosity respectively. Values of these parameters were taken as for water at 293 K.

During one PLIF or PIV measurement, 2000 two-dimensional maps of tracer concentration and two components of velocity vector respectively were acquired. The areas of the mixers were divided into several parts which covered completely the whole mixing zone within the mixers. Mean values were calculated from the 2000 instantaneous data. The velocity value was calculated from the values of two components of the velocity vector.

Figures 3 and 4 show measured and predicted contours of mean velocity in two of the studied mixers. In the case of T-mixer I the Figure 3 shows simulation results for k-ε and LES models for Re_{jet} = 2000 and Re_{jet} = 4000, whereas Figure 4 presents the results for V-mixer I for Re_{jet} = 1000 and Re_{jet} = 2000.

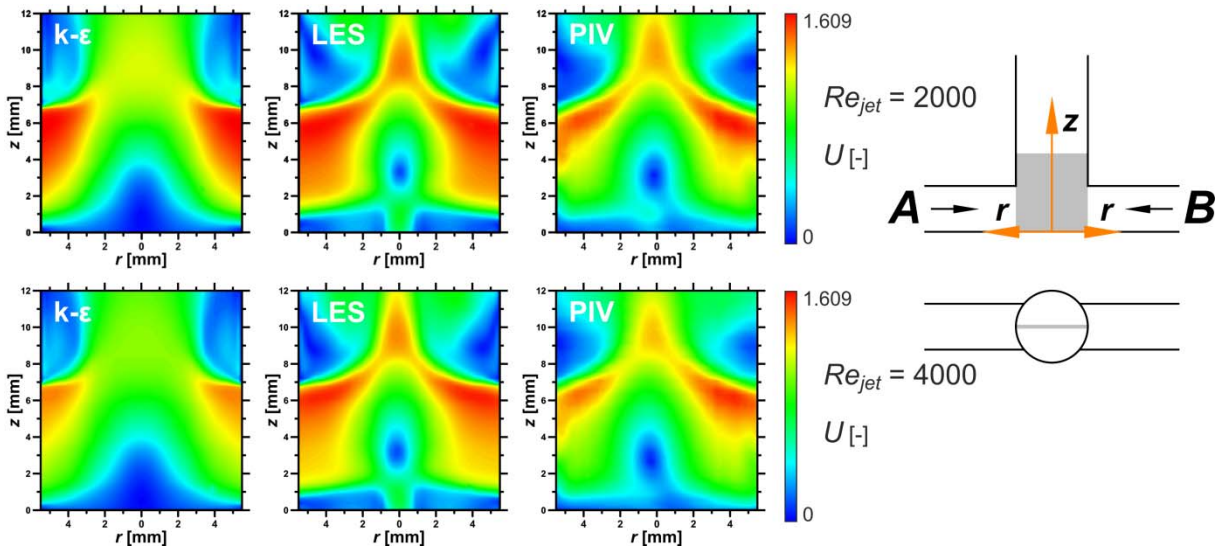

Fig. 3. Contours of the measured and predicted values of the dimensionless velocity magnitude in T-mixer I in injection zone. U is a ratio of the local mean velocity to mean velocity in the inlet pipe, u_{jet}

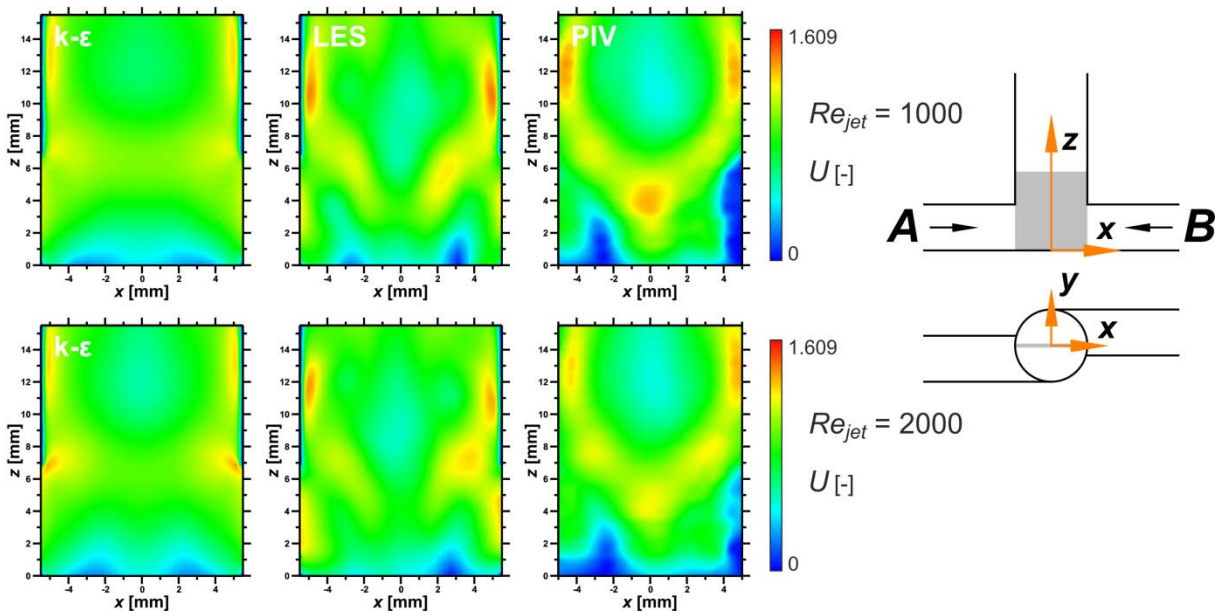

Fig. 4. Contours of the measured and predicted values of the dimensionless velocity magnitude in the V-mixer I in injection zone, y=0 mm. U is a ratio of the local mean velocity to mean velocity in the inlet pipe, u_{jet}

Figure 5 shows distributions of dimensionless mean velocity in T-mixer I. One can see that the agreement between experimental and simulation results in the region of impingement is better for the large eddy simulation than that for the k-ε model, especially for a lower tested value of Reynolds number. As for high values of Re_{jet}, both models predict results which are in good agreement with experiments. It results from the theory of the k-ε model that was developed for fully turbulent flow.

Figure 6 presents measured and calculated contours of dimensionless axial root-mean-square velocity fluctuations $U_{z,RMS}$. The results from k-ε model were calculated from the kinetic energy of turbulence $u_{z,RMS} = \sqrt{2/3k}$. The comparison shows a much better agreement of the LES results with the experimental data than the results of the k-ε model.

The collected data from PLIF experiments, after numerical and statistical analysis, allowed to determine the mixture fraction for the two mixed fluids. The contours of mean mixture fraction for T-mixer I are shown in the Figure 7, whereas Figure 8 shows the contours of mean mixture fraction in V-mixer I.

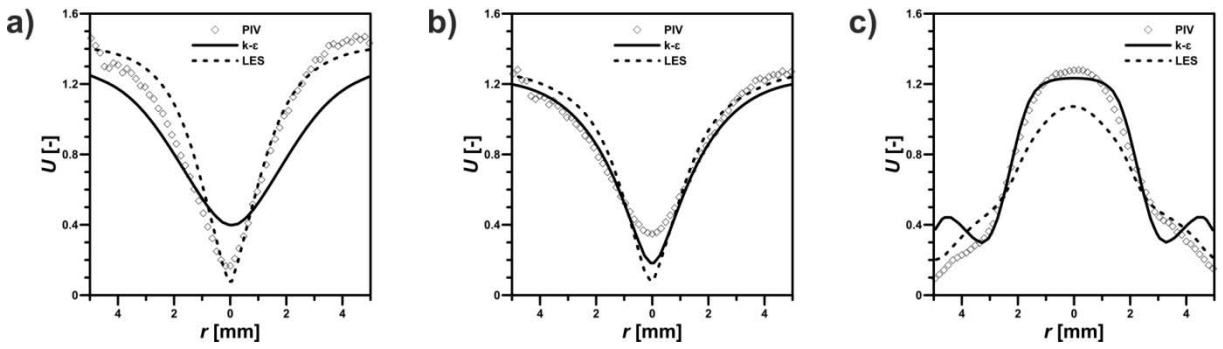

Fig. 5. Dimensionless mean velocity distributions on the axis of inlet jets, T-mixer I: a) Re_{jet}=1000, z=3.5 mm; b) Re_{jet} = 4000, z = 3.5 mm; c) Re_{jet} = 4000, z = 8.5 mm. U is a ratio of the local mean velocity to mean velocity in the inlet pipe, u_{jet}

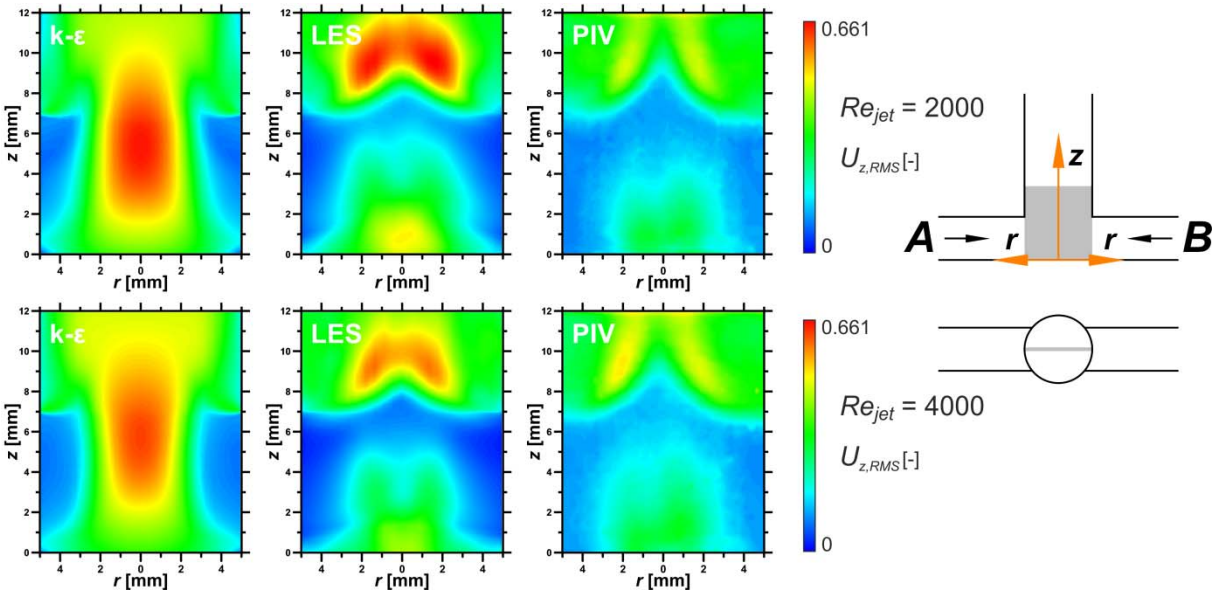

Fig. 6. Contours of the measured and predicted values of dimensionless root-mean-square velocity fluctuations, $U_{z,RMS}$, in the T-mixer I in injection zone. $U_{z,RMS}$ is a ratio of the local root-mean-square velocity fluctuations to mean velocity in the inlet pipe, u_{jet}

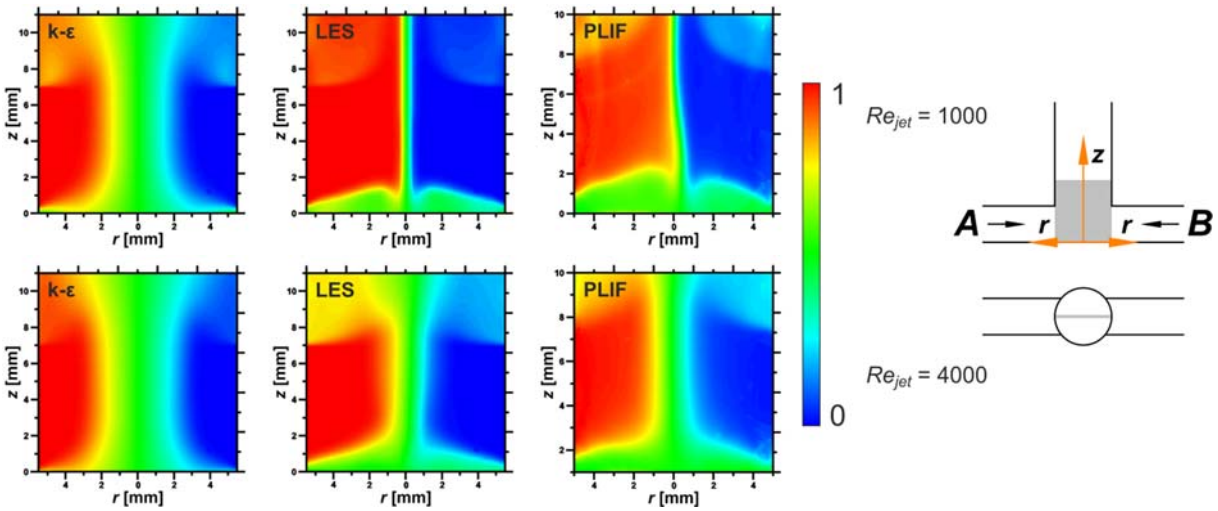

Fig. 7. Contours of the measured and predicted values of mean mixture fraction in T-mixer I

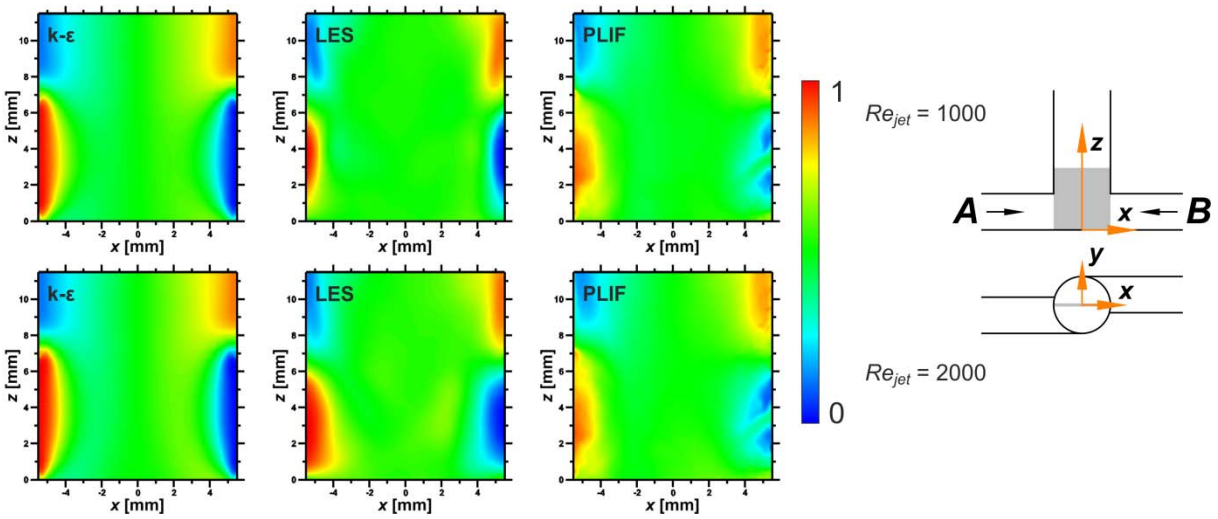

Fig. 8. Contours of the measured and predicted values of mean mixture fraction in V-mixer I, y = 0 mm

For T-mixer I, the *k*-ε model again is not working properly, because it predicts faster mixing than that observed in experiments. For a high tested Reynolds number the compliance is slightly better, because RANS models were developed for a fully turbulent flow. However, LES gives results more similar to the experiments across the tested range. In case of V-mixer I both model predictions give tendencies observed in the experiments, which can be explained by increased vorticity and turbulence in the impingement zone in this type of mixer. This is shown in Figure 9, which presents mean mixture fraction distributions along inlet jets axis in both studied mixers.

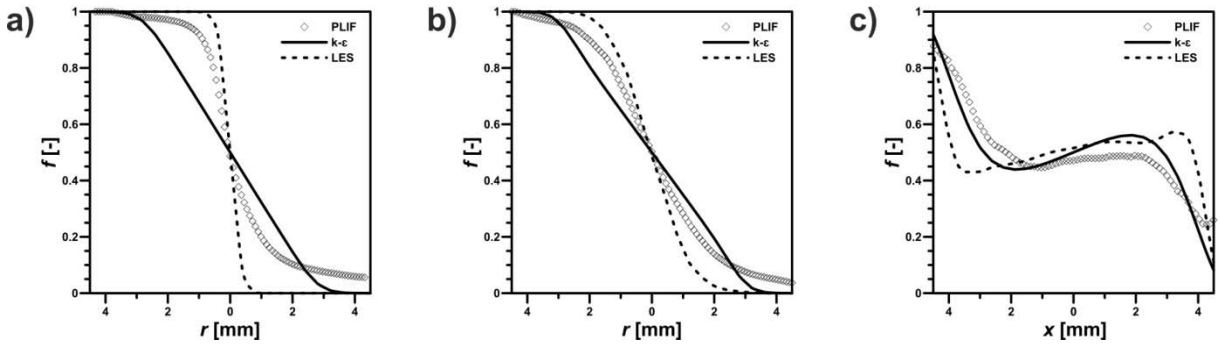

Fig. 9. Mean mixture fraction distributions on the axis of inlet jets, d_{jet} = 7 mm, z = 3.5 mm: a) T-mixer I, Re_{jet} = 1000; b) T-mixer I, Re_{jet} = 4000; c) V-mixer I, Re_{jet} = 4000, y = 0 mm

In the case of smaller jet mixers (T-mixer II), the *k*-ε model also gives incorrect results. Figure 10 shows that even for a relatively high Re_{jet} the model does not simulate properly fluid behaviour in the mixing chamber, since it fails to predict generation of vortices due to collision of inlet streams. This follows from the theory of turbulence models and is related to Reynolds-averaged approach, in which resolving all spatial and temporal small-scale phenomena is not necessary since the variation of time-averaged quantities occurs at much larger scales (Ranade, 2002). LES again gives results much more similar to experiments. In case of V-mixer II both models give a good agreement with experimental data.

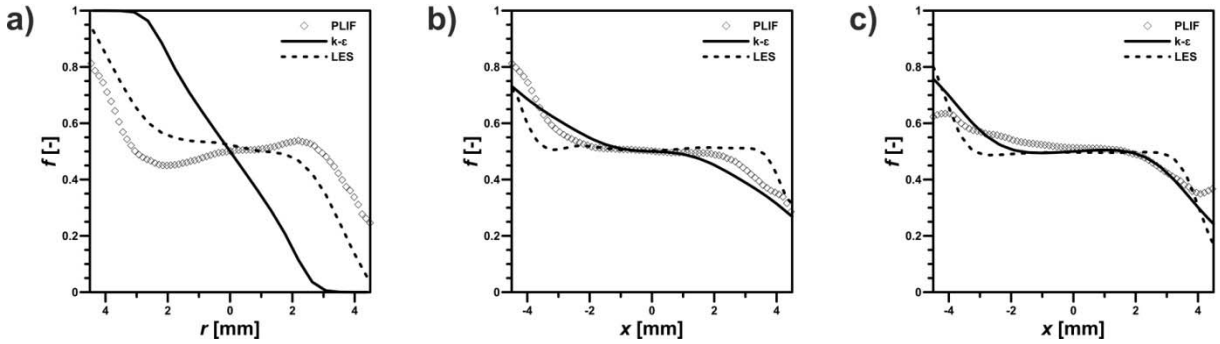

Fig. 10. Mean mixture fraction distributions on the axis of inlet jets, d_{jet} = 4.6 mm: a) T-mixer II, Re_{jet} = 4000, z = 2.3 mm; b) V-mixer II, Re_{jet} = 1000, z = 7.3 mm, y = 0 mm; c) V-mixer II, Re_{jet} = 4000, z = 2.3 mm, y = 0 mm

Figure 11 shows examples of instantaneous contours of mixture fraction in T-mixer I. One can clearly see differences between the instantaneous and time averaged values, and a good agreement of both model predictions with experimental data. In case of V-mixer II, one can see that LES gives a slightly better agreement with experiments, because it properly simulates eddy behaviour along the outlet pipe, while the *k*-ε model overestimates mixing intensity and speed.

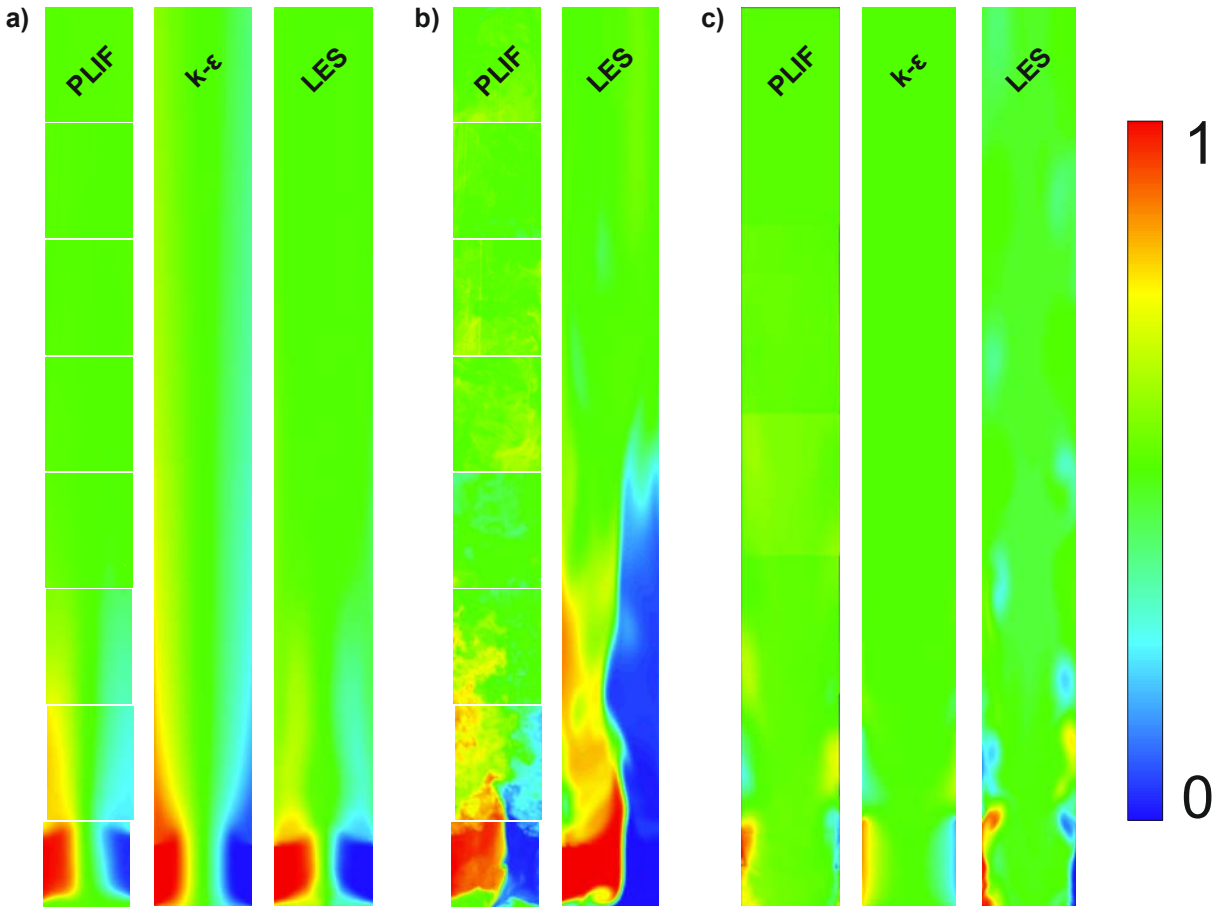

Fig. 11. Contours of the measured and predicted instantaneous and mean values of the mixture fraction in: a) T-mixer I, $Re_{jet} = 4000$, mean values; b) T-mixer I, $Re_{jet} = 4000$, instantaneous values; c) V-mixer II, $Re_{jet} = 1000$, mean values

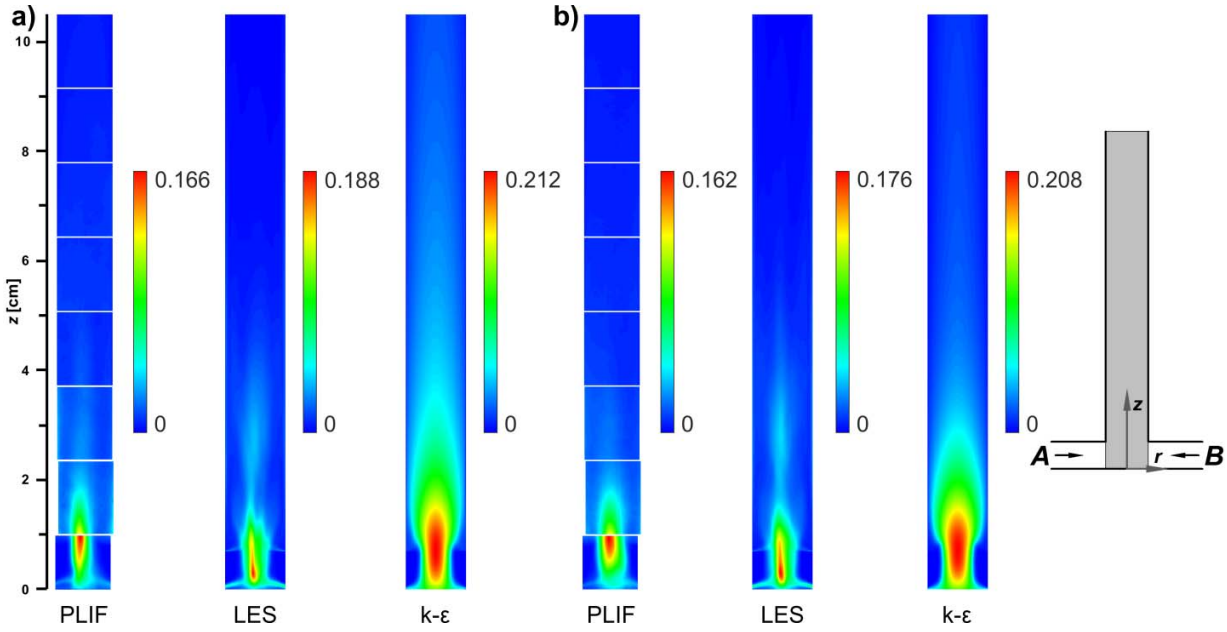

Fig. 12. Contours of mean mixture fraction variance in T-mixer I: a) $Re_{jet} = 2000$; b) $Re_{jet} = 4000$

Figure 12 shows the mixture fraction variance contours in the T-mixer I for $Re_{jet} = 2000$ and $Re_{jet} = 4000$. One can see that both models overestimate the experimentally determined variance.

However, for a higher tested Reynolds number overestimation resulting from the application of the scale-similarity model (Cook and Riley, 1994; Michioka and Komori, 2004), is smaller, and the model gives the best prediction of the variance contours in the system. One can see that with increasing turbulence intensity, the model tends to give more accurate results. The possible reason for such behaviour is that the constant coefficient in the model was estimated for a fully developed turbulent flow. However, in the system there is a significant spatial variation of turbulence intensity.

Figure 13 shows variance distributions in the impingement zone in T-mixer I. One can clearly see that LES gives the best predictions of mixing in terms of the position in which mixing occurs.

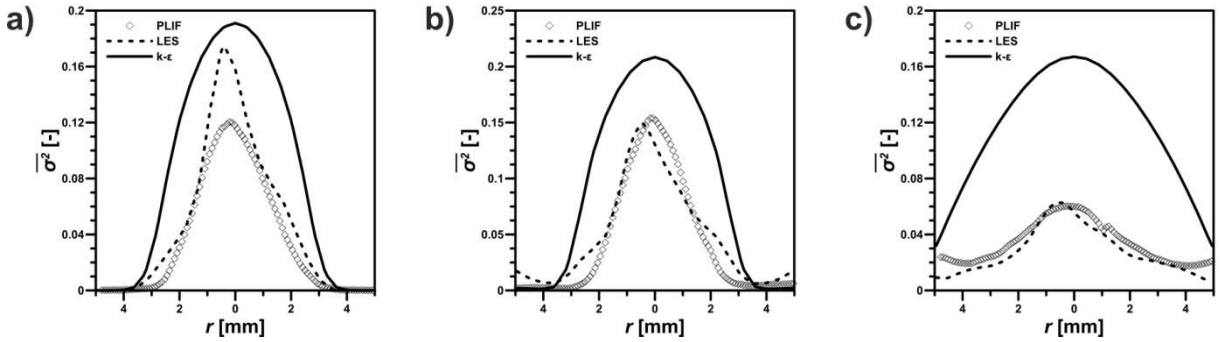

Fig. 13. Mean mixture fraction variance distributions in T-mixer I, Re_{jet} = 4000: a) z = 3.5 mm; b) z = 7 mm; c) z = 13.5 mm

In Figure 14 one can see variance distributions in the impingement zone in T-mixer II. In this mixer, k-ε predictions completely differ from measurements, both with variance values and position in which mixing occurs. As was discussed above, this results from the theory of the k-ε model supplemented with a turbulent mixer model, which was developed for a fully turbulent flow. Despite the overestimation of maximum variance values, LES predicts well the shape of the variance distribution in the system, especially for higher tested values of Re_{jet}.

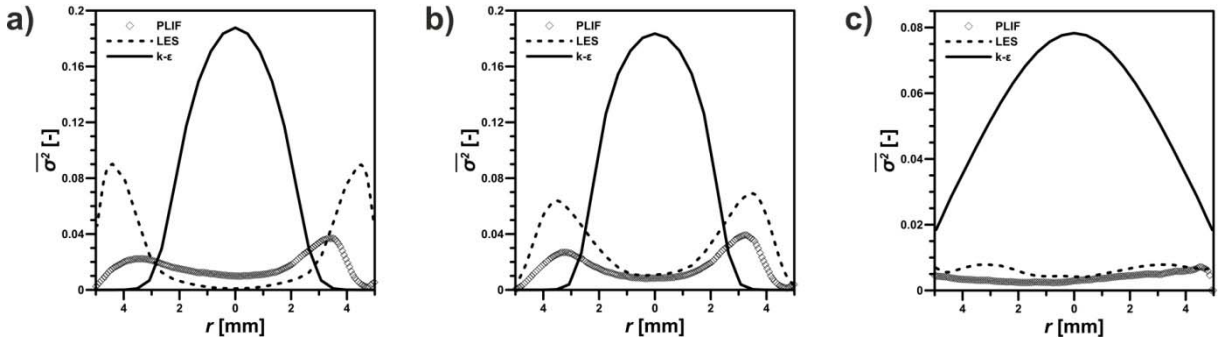

Fig. 14. Mean mixture fraction variance distributions in T-mixer II, d_{jet} = 4.6 mm: a) Re_{jet} = 1000, z = 2.3 mm; b) Re_{jet} = 4000, z = 2.3 mm; c) Re_{jet} = 4000, z = 12.3 mm

The results of large eddy simulation may depend on a model of concentration variance used in computations. The value of the constant c_L in Equation (5) is 5.0 in the modeling of high-Schmidt number liquid flows. Since the value can also change with the numerical grid scale size, Δ, which should lie in the inertial-convective subrange of energy spectrum, it is necessary to develop passive tracer concentration variance models, especially with a dynamic method to determine the model coefficient.

5. CONCLUSIONS

In this work PIV and PLIF techniques were applied to measure instantaneous and mean distributions of velocity and tracer concentration in impinging jet mixers. In recent years these types of reactors have been used more and more often in the production of nanocrystals due to their very good mixing conditions. It should be noted that the recently published studies of the mixing process in this type of mixers not only focus on microreactors, but increasingly also on larger jet reactors (from hundreds of micrometers to a few millimeters) in which flow instabilities and large scale inhomogeneities give a positive influence on the turbulent mixing process. Performed experiments were compared with RANS and LES model predictions. Presented results show that both models gave similar results for higher tested values of Reynolds number and were in a good agreement with the experiments. In case of lower tested values of Reynolds number, especially in two symmetric mixers, LES results were more similar to experimental data than RANS (k-ε) results, which shows the importance of effects of large scale inhomogeneities that are predicted by LES and neglected by RANS. Differences between simulation results and experimental data of concentration variance are clearly visible. However, the shape of variance distribution, which corresponds to the area of mixing, obtained by the LES is well predicted. A possible improvement in LES modelling of complex chemical processes is to develop a new model for concentration variance, which would take into account the local variation of the turbulence Reynolds number, the Schmidt number and the numerical cell size. In modelling of the course of complex chemical processes it is very important to determine correctly the reaction zone which is directly linked to the mixing zone. This study confirmed the usefulness of large eddy simulation in the whole studied range of jet Reynolds numbers.

This work was supported by the by National Science Centre (Decision No DEC-2013/09/B/ST8/02869).

SYMBOLS

c	tracer concentration, g/m^3
c_L	model constant
d_{jet}	inlet pipe diameter, mm
d_{out}	outlet pipe diameter, mm
D_m	molecular diffusivity, m^2/s
D_{sgs}	subgrid scale diffusivity, m^2/s
f	dimensionless tracer concentration
k	turbulence kinetic energy, m^2/s^2
N	number of images
Re_{jet}	Reynolds number
U	dimensionless mean velocity
u_{jet}	mean inlet velocity, m/s
$U_{z,RMS}$	dimensionless root-mean-square velocity fluctuations
$u_{z,RMS}$	root-mean-square velocity fluctuations, m/s

Greek symbols

Δ	mean filter width, m
ε	turbulence kinetic energy dissipation rate, m^2/s^3
μ	dynamic viscosity, Pas
ρ	density, kg/m^3
σ^2	tracer concentration variance
τ	mean residence time, s

REFERENCES

Bałdyga J., 1989. Turbulent mixer model with application to homogeneous, instantaneous chemical reactions. *Chem. Eng. Sci.*, 44, 1175-1182. DOI: 10.1016/0009-2509(89)87016-2.

Bałdyga J., Bourne J.R., 1999. *Turbulent mixing and chemical reactions*. Wiley, Chichester.

Cook A. W., Riley J.J., 1994. A subgrid model for equilibrium chemistry in turbulent flows. *Phys. Fluids*, 6, 2868-2870. DOI: 10.1063/1.868111.

Icardi M., Gavi E., Marchisio D.L., Olsen M.G., Fox R.O., Lakehal D., 2011. Validation of LES predictions for turbulent flow in a Confined Impinging Jets Reactor. *Appl. Math. Modell.*, 35, 1591-1602. DOI: 10.1016/j.apm.2010.09.035.

Johnson B.K., Prud'homme R.K., 2003. Chemical processing and micromixing in confined impinging jets. *AIChE J.*, 49, 2264-2282. DOI: 10.1002/aic.690490905.

Kölbl A., Kraut M., Wenka A., 2011. Design parameter studies on cyclone type mixers. *Chem. Eng. J.*, 167, 444-454. DOI: 10.1016/j.cej.2010.08.092.

Lince F., Marchisio D.L., Barresi A.A., 2008. Strategies to control the particle size distribution of poly-ε-caprolactone nanoparticles for pharmaceutical applications. *J. Colloid Interface Sci.*, 322, 505-515. DOI: 10.1016/j.jcis.2008.03.033.

Liu Y., Cheng C., Prud'homme R.K., Fox R.O., 2008. Mixing in a multi-inlet vortex mixer (MIVM) for flash nano-precipitation. *Chem. Eng. Sci.*, 63, 2829-2842. DOI: 10.1016/j.ces.2007.10.020.

Makowski Ł., Bałdyga J., 2011. Large Eddy Simulation of mixing effects on the course of parallel chemical reactions and comparison with k–ε modeling. *Chem. Eng.Process*, 50, 1035-1040. DOI: 10.1016/j.cep.2011.06.003.

Makowski Ł., Orciuch W., Bałdyga J., 2012. Large eddy simulations of mixing effects on the course of precipitation process. *Chem. Eng. Sci.*, 77, 85-94. DOI: 10.1016/j.ces.2011.12.020.

Marchisio D.L., 2009. Large Eddy Simulation of mixing and reaction in a Confined Impinging Jets Reactor. *Comput. Chem. Eng.*, 33, 408-420. DOI: 10.1016/j.compchemeng.2008.11.009.

Michioka T., Komori S., 2004. Large-Eddy simulation of a turbulent reacting liquid flow. *AIChE J.*, 50, 2705-2720. DOI: 10.1002/aic.10218.

Midler M., Paul E.L., Whittington E.F., Futran M., Liu P.D., Hsu J., Pan S.H., 1994. *US Patent 5 314 506*.

Mortensen M., Orciuch W., Bouaifi M., Andersson B., 2004. Mixing of a jet in a pipe. *Chem. Eng. Res. Des.*, 82, 357-363. DOI: 10.1205/026387604322870462.

Pitsch H., Steiner H., 2000. Large-eddy simulation of a turbulent piloted methane/air diffusion flame (Sandia flame D). *Phys. Fluids*, 12, 2541-2554. DOI: 10.1063/1.1288493.

Pope S. B., 2004. Ten questions concerning the large-eddy simulation of turbulent flows. *New J. Phys.*, 6, 35. DOI: 10.1088/1367-2630/6/1/035.

Ranade V.V., 2002. *Computational flow modeling for chemical reactor engineering*. Academic Press, California.

Santillo G., Deorsola F.A., Bensaid S., Russo N., Fino D., 2012. MoS_2 nanoparticle precipitation in turbulent micromixers. *Chem. Eng. J.,* 207-208, 322-328,. DOI: 10.1016/j.cej.2012.06.127.

Schwertfirm F., Manhart M., 2010. A numerical approach for simulation of turbulent mixing and chemical reaction at high Schmidt numbers, In: Bockhorn H., Mewes D., Peukert W., Warnecke H.J. (Eds.), *Micro and Macro Mixing*. Springer-Verlag, Berlin, 305-324.

A. Tamir, 1994. *Impinging-Stream Reactors*. Elsevier Science B.V., Amsterdam.

Received 01 April 2015
Received in revised form 01 June 2015
Accepted 01 June 2015